Journal of Inorganic and Organometallic Polymers and Materials
https://doi.org/10.1007/s10904-020-01558-x

Partially Exfoliated α-ZrP Reinforced Unsaturated Polyester Nanocomposites by Simultaneous Co-polymerization and Brønsted Acid–Base Strategy

Prabunathan Pichaimani[1] · Hariharan Arumugam[1] · Dineshkumar Gopalakrishnan[2] · Balaji Krishnasam[1] · Alagar Muthukaruppan[1]

Received: 25 February 2020 / Revised: 9 April 2020 / Accepted: 24 April 2020

Abstract
In the present work, allylamine exfoliated alpha zirconium phosphate (A_XZrP) reinforced unsaturated polyester (UP) nanocomposites were developed and characterized. Exfoliation of alpha zirconium phosphate (α-ZrP) was achieved through Brønsted acid–base interaction using allylamine in different mole ratios. The partially exfoliated α-ZrP possesses a higher concentration of α-ZrP than completely exfoliated. Subsequently, the partially exfoliated α-ZrP was reinforced with UP resin to enhance the thermal and mechanical properties of the resulting composite. Detailed studies using scanning electron microscopic and X-ray diffraction analysis suggest that the A_XZrP/UP composite possesses a homogeneous distribution of α-ZrP within the UP matrices. For 10.0 wt% A_XZrP/UP composite, the mechanical properties such as tensile and flexural strength were observed to enhance up to 56% and 61% respectively. Further, appreciable enhancement in the flame retardant behavior with V0 rating and high thermal stability with LOI value of 27.1% for 10.0 wt% A_XZrP/UP composite was observed. Similarly, the catalytic effect of α-ZrP contributes to enhancing the flame retardant behavior along with rapid char formation.

Keywords α-ZrP · Exfoliation · Unsaturated polyester · Thermal · Mechanical properties · Composites

1 Introduction

Unsaturated polyester (UP) resins have been used extensively in industrial applications such as aerospace, automotive, naval constructions, coatings and load-bearing composites [1–4]. Particularly, the excellent mechanical, electrical, and chemical resistant properties of UP resins from low-cost processability led to its inevitable in industrial applications [5–7]. However, the high potential utility of UP resin has been limitedly explored due to high flammability with dripping and a huge density of toxic smoke. In this context, the incorporation of intumescent halogen-free inorganic particles with UP resins promotes the flame retardant nature to an appreciable extent [8–10]. Particularly, the incorporation of additive-type flame retardants catalyzes the rapid char formation via acid donor mechanism, and reduce smoke [11–13].

The advancements of new polymer nanocomposites using nanostructures reinforcement have been studied extensively due to their multifunctional nature [14–19]. Particularly, the high aspect ratio and heat bearing capacity of layered nanofillers such as montmorillonite (MMT) clay, layered hydroxides (LDHs), ammonium phosphates (APPs) and alpha-zirconium phosphates (α-ZrP) show a significant role in advanced composites [20–23]. Similarly, the distribution of the layered fillers displays a strong role in tailoring the thermal barrier, mechanical properties of polymeric materials. The utility of MMT, LDH, and APP is limited due to the nature of physical interaction, less distribution, high cost, and liberation of volatiles [24–26]. In this background, an

Electronic supplementary material The online version of this article (https://doi.org/10.1007/s10904-020-01558-x) contains supplementary material, which is available to authorized users.

✉ Prabunathan Pichaimani
nanonathan@gmail.com

✉ Alagar Muthukaruppan
mkalagar@yahoo.com

[1] Polymer Engineering Laboratory, PSG Institute of Technology and Applied Research, Coimbatore 641 062, India

[2] Department of Chemistry, PSG College of Arts and Science, Coimbatore 641 014, India

Published online: 30 April 2020

alternately layered filler providing chemical interaction and homogenous distribution without emission is still in high demand.

Layered zirconia phosphates and silicates were used in many applications in biodiesel, agriculture and industrial processes [27, 28]. The alpha zirconium phosphate (α-ZrP) with acid groups on the surface layers allows direct intercalation of a variety of substances, particularly alkyl amines [29, 30]. α-ZrP forms lamellar morphology on exfoliation through Brønsted acid–base interaction with varieties of amines [31]. This versatile behavior of α-ZrP finds a wide range of applications such as ion-exchange [32, 33], flame retardant [34], catalyst [35], adsorbent [36], sensor [28] and reinforcement [37]. Inherent higher thermal stability and flame retardancy of α-ZrP offers unavoidable candidature as filler to promote properties of polymeric materials [22, 38]. In this context, Cai et al. (2013) achieved V0 rating for polystyrene using the silylated zirconium phosphate (α-ZrP) as the flame retard filler [39]. So far, no significant attempt has been made to study the flame retardant behavior of unsaturated polyester resin using α-ZrP with suitable modification.

Thus, the inspiring properties of α-ZrP and our continuous interest in high-performance UP composites made to study the thermo-mechanical properties of α-ZrP reinforced UP nanocomposites. Herein, the present work studies the exfoliation behavior of α-ZrP with different concentrations of allylamine and their impact on properties of the UP matric on reinforcing. Besides, the compatibility of α-ZrP with the UP resin was studied by using allylamine as both exfoliator and cross-linker. The Brønsted acid-base interaction between amine and α-ZrP, followed by co-polymerization of allyl group with UP resin could impart homogeneous distribution of reinforcement to promote the thermal and mechanical behavior. Though different studies were reported about the exfoliation character of α-ZrP using different alkyl amines, no significant interest is paved to use allylamine as both an exfoliator and cross-linker.

2 Experimental

2.1 Materials

Zirconyl chloride octahydrate is purchased from Sigma Aldrich, India. Phosphoric acid, allylamine, DMF and benzoyl peroxide were purchased from SRL (India). The unsaturated polyester resin was received from Ciba-Geigy Ltd.

2.2 Preparation of Alpha Zirconium Phosphate (α-ZrP)

Alpha zirconium phosphate (α-ZrP) was synthesized as per the reported procedure [40]. 4.0 g $ZrOCl_2 \cdot 8H_2O$ was mixed with 40.0 mL of 12.0 M H_3PO_4 and sealed into a Teflon-lined pressure vessel and heated at 200 °C for 24 h and then cooled. Once, the autoclave reached room temperature, the resulting white powder of ZrP was separated by centrifugation and the powder was repeatedly washed with DI water three times and filtered. Then the sample is dried in an oven at 70 °C overnight and ground into fine powder for further use.

2.3 Exfoliation of Alpha Zirconium Phosphate (α-ZrP)

Exfoliation of α-ZrP in water was performed using allylamine as an intercalating agent [41]. Initially, two sets of α-ZrP suspension containing 0.5 g α-ZrP (0.7 mmol) in 33 mL water were prepared through sonication. 16.6 mL of 0.1 and 0.05 M allylamine were added individually to the different vessels containing α-ZrP suspension and allowed to stir for another 24 h. Further, both mixtures were subjected to ultrasonication for another 6 h and then treated with 6 mL of 1 M HCl (pH < 2) to regenerate the protonated form of zirconium phosphates. The formed gelatinous precipitates were settled by centrifugation at 3000 rpm and subsequently washed with deionized water to remove chloride ions. Finally, the hydrated gels were washed repeatedly with an excess of DMF to remove the water. The resulted gels (A_xZrP) obtained using 0.05 and 0.1 M allylamines are referred to as $A_{0.5}$ZrP and $A_{1.0}$ZrP respectively.

2.4 Preparation of $A_{0.5}$ZrP/UP Nanocomposites

100 parts of unsaturated polyester resin and different weight percentages of $A_{0.5}$ZrP (0, 1.0, 2.5, 5.0, 7.5 & 10 wt%) were separately mixed and agitated using mechanical stirrer for 12 h to obtain homogeneity in distribution. Then, the 0.5 g of benzoyl peroxide was added and subsequently agitated for another 30 min. The observed product resulted was subjected to vacuum to remove the trapped air and then poured into a preheated mold to cast, and cured at 110 °C for 2 h and post-cured at 150 °C for 3 h. Finally, the resulted neat matrix and composites with different weight percentages of A_xZrP/UP were removed from the mold and preserved for further characterization (Fig. 1).

2.5 Characterization

Fourier transform infrared (FT-IR) spectra were recorded on a Thermo-scientific Nicolet 6700-FTIR spectrometer. The XPS was measured using an Omicron nanotechnology instrument at a pressure below 10^{-10} Torr. The curing and thermal properties were determined using TGA-DSC NETZSCH STA 449F3 Jupiter-German. The flame retardant behavior of the materials can be analyzed from

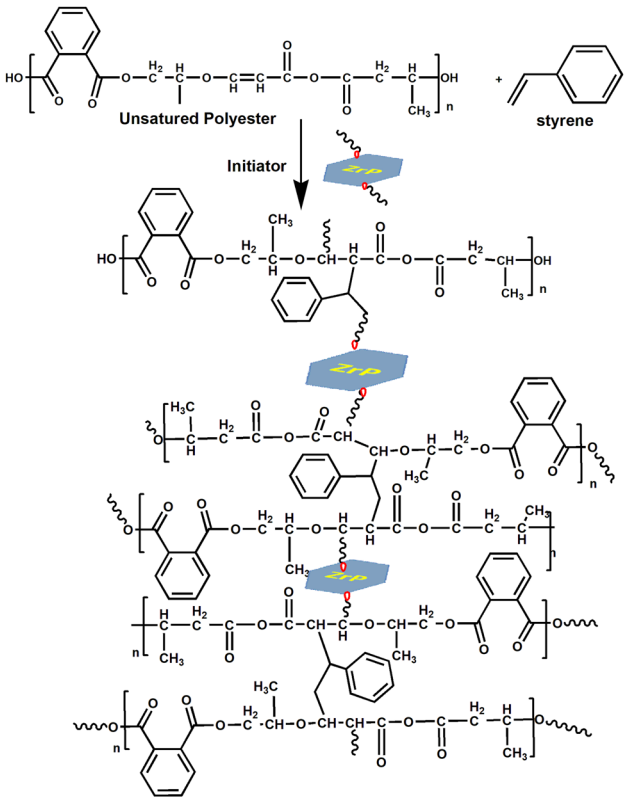

Fig. 1 Schematic representation of formation of allyl amine exfoliated ZrP reinforced UP nanocomposites

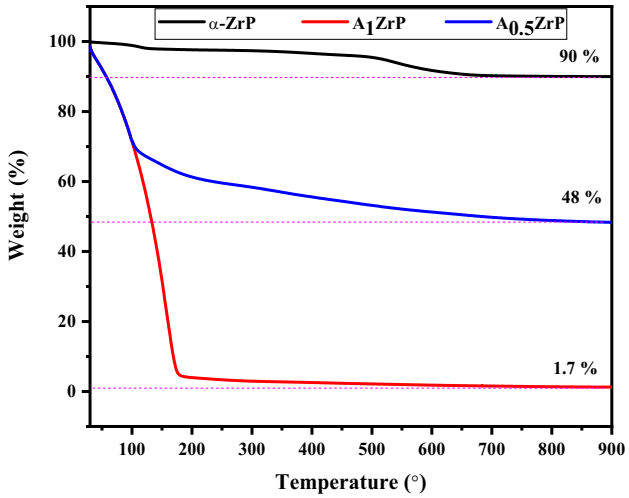

Fig. 2 TGA curve of α-ZrP and allyl amines exfoliated α-ZrP

the value of the Limiting Oxygen Index (LOI). Van Krevelen and Hoftyzer relation based on LOI and char yield (LOI = 17.5 + 0.4 CR) are generally used to calculate the value of LOI [42]. The tensile property was determined using Instron (Model 6025 UK) as per ASTM D 3039. Flexural strength was determined based on ASTM D 7264. X-ray diffraction patterns were recorded at room temperature, by monitoring the diffraction angle 2θ from 10 to 80° on a PAN analytical X'pert3 powder - Netherlands. The surface morphology of the samples was examined FESEM Zeiss Zigma Gemini 0336 – USA, attached with EDX - Bruker nano X flash - German. Flame retardancy was analysed based on UL-94 standards. HR-TEM images were captured using a Tecnai G2 S-Twin high-resolution transmission electron microscope.

3 Results and Discussion

3.1 Characterization of α-ZrP and A_xZrP

Thermogravimetric analysis (TGA) was performed to determine the quantity of α-ZrP present in the exfoliated samples namely $A_{1.0}$ZrP and $A_{0.5}$ZrP. The thermograms of α-ZrP, $A_{1.0}$ZrP and $A_{0.5}$ZrP are presented in Fig. 2. In Fig. 2, at 900 °C, only 10% weight loss was observed for the α-ZrP whereas about 52.0 and 98.3% weight loss was observed for $A_{0.5}$ZrP and $A_{1.0}$ZrP samples respectively. The weight loss for α-ZrP occurs in two stages, the first stage degradation occurring from 100 to 170 °C corresponds to the loss of crystallization water present in between the hexagonal platelets. The second stage degradation observed from 420 to 600 °C, corresponds to the formation of polyphosphates through dehydration and condensation of P–OH [38, 43]. However, both exfoliated samples namely $A_{0.5}$ZrP and $A_{1.0}$ZrP show major weight losses below 170 °C due to the decomposition of allylamines. After 900 °C, the $A_{0.5}$ZrP and $A_{1.0}$ZrP afforded 48 and 1.7 wt% respectively, whereas the α-ZrP left 90 wt% residue. Because of the presence of a higher amount of α-ZrP in the $A_{0.5}$ZrP sample compared to $A_{1.0}$ZrP, the $A_{0.5}$ZrP is further used as reinforcement.

Further, the X-ray diffraction analysis was carried out to validate the formation and exfoliation of α-ZrP. The diffractogram of α-ZrP and $A_{0.5}$ZrP are presented in Fig. 3. The peak appeared at 11.7° corresponds to the (002) plane of α-ZrP with a basal interlayer spacing of 7.6 Å. Further, the peaks appeared at 19.8° and 24.9° corresponding to the (110) and (112) planes of α-ZrP respectively. It is important to note that the relative peak intensity of (110) and (112) planes are equivalent due to addition of high concentration (12 M) of phosphoric acid during hydrothermal synthesis, in which the growth mechanism of α-ZrP occurs rapidly. The sharp and intense diffraction patterns of α-ZrP confirm the formation of ZrP possessing alpha phase, which is highly crystalline with a high aspect ratio The diffraction pattern is found to be in accordance with JCPDS card no. 34–0127 [44, 45]. However, the XRD pattern of $A_{0.5}$ZrP present in Fig. 3 shows only a broad peak at 22.4° and confirms the

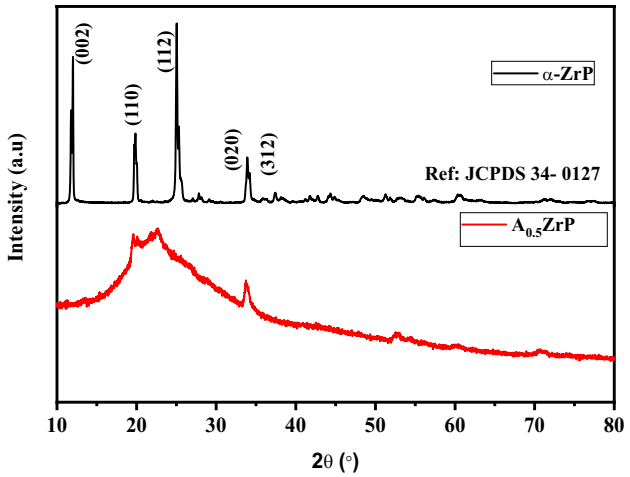

Fig. 3 XRD patterns of α-ZrP and allyl amine exfoliated α-ZrP

occurrence of exfoliation of layered structure results in less ordered amorphous behavior rather than crystalline [30, 35, 46].The proposed schematic illustration of the intercalation mechanism is shown in Fig. 4. The partial exfoliation of α-ZrP with allylamine could be attributed to the intercalation of short chains and less polar nature of allylamine when compared to the previously reported alkyl amine substrates [47, 48].

The field emission scanning electron microscope analysis was performed to analyze the surface morphology of both α-ZrP and $A_{0.5}$ZrP samples and depicted in Fig. 5. From Fig. 5a–c, it can be seen that the α-ZrP possesses a layered hexagonal morphology. The α-ZrP shows smooth surfaces with narrow size distribution and high aspect ratio as similar to previous reports [49]. To enhance the functional properties of polymers using layered structure, the narrow size distribution is highly warranted. The morphology of the exfoliated $A_{0.5}$ZrP is also presented in Fig. 5d–g. Interestingly, a single layer hexagonal morphology of $A_{0.5}$ZrP is seen in a high magnified micrograph (Fig. 5f–g). A single layer of $A_{0.5}$ZrP with rough surface forming cluster-like appearance in Fig. 5g confirms the presence of pillared allyl amines on the surfaces of α-ZrP. Thus, the Brønsted acid-base interaction between allylamine and α-ZrP leads to partial exfoliation of hexagonal structured α-ZrP, which is an essential condition for further reinforcing with unsaturated polyester resin. Further, the elemental mapping analysis presented in Fig. 5h, i confirms the presence of Zr (red) and P (green) in the exfoliated $A_{0.5}$ZrP. Also, the EDS of the ZrP is given in the supporting information Figure S1. The atomic percentage of oxygen, phosphorus and zirconium observed are 63.18, 21.07 and 15.75% respectively.

To substantiate the results of SEM and XRD, FTIR and XPS analysis were carried out for both α-ZrP and $A_{0.5}$ZrP samples and presented in Fig. 6a, b respectively. In the FTIR spectra of α-ZrP, the peaks appeared at 1248, 1068, and 968 cm^{-1} corresponds to the asymmetric and symmetric vibrations of the phosphate functional groups (for clarity see inset of Fig. 6) [50]. Besides, the FTIR of $A_{0.5}$ZrP exhibits a new peak at 3441 cm^{-1} correspondings to the N–H vibrations of an amine functional group pillared on the surfaces of ZrP. Further, the peaks appeared

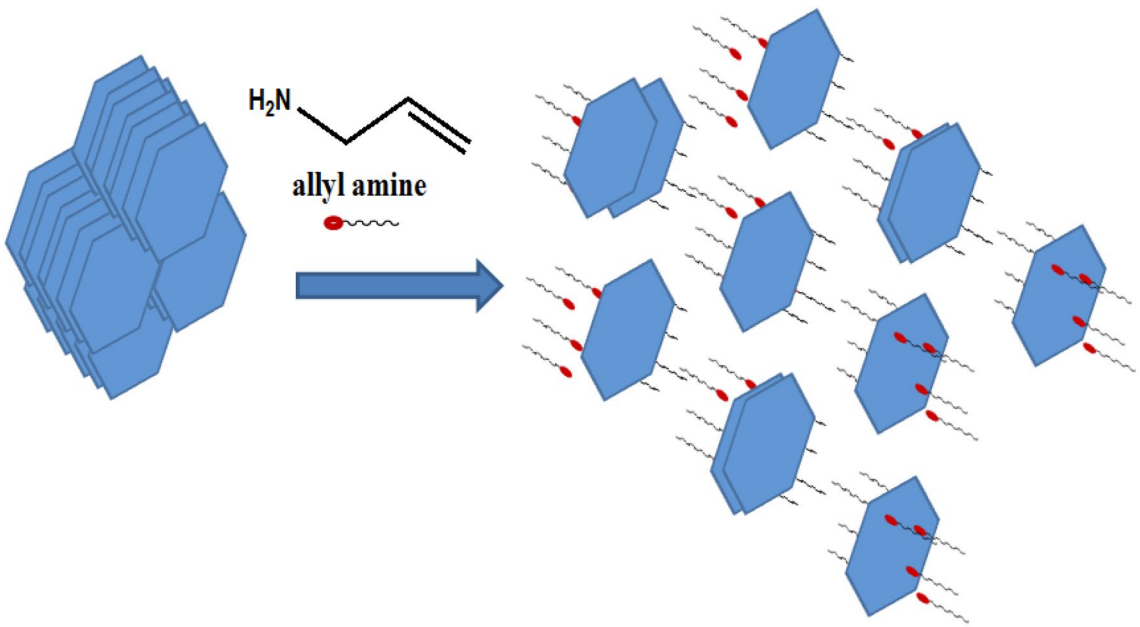

Fig. 4 Schematic representation of intercalation of allyl amine within layered α-ZrP

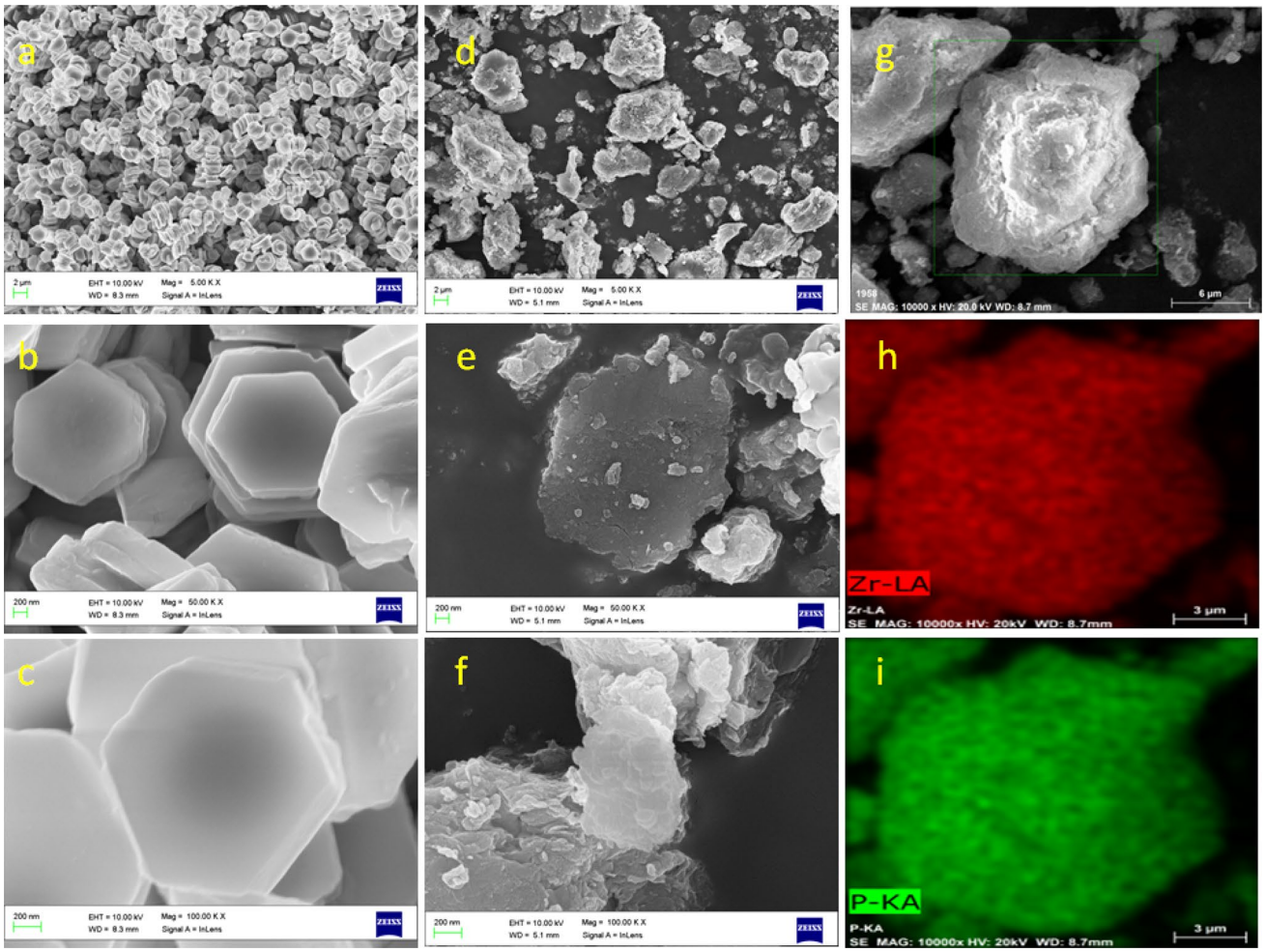

Fig. 5 **a–c** SEM micrograph of α-ZrP at different magnification, **d–g** SEM micrograph of allyl amine exfoliated α-ZrP at different magnification and **h–i** elemental mapping of Zr and P present in exfoliated ZrP

at 2942 and 2872 cm^{-1} corresponds to the $–CH_2–$ vibrations present in the allyl chain. However, the vibrations of phosphate functional groups of $A_{0.5}ZrP$ are shifted to the lower region and thus the peaks tend to appear at 1009 and 864 cm^{-1} [39]. This phenomenon confirms the occurrence of intercalation of allylamine between the layers of α-ZrP and exfoliates [29]. The peaks appeared at 1498 and 1648 cm^{-1} corresponds to the asymmetric and symmetric stretching of formed $^{+}NH_3$ ionic structure via Brønsted acid–base interaction of P–OH and NH_2 [50]. Figure 6b shows the XPS binding energy curve of $A_{0.5}ZrP$. The presence of elements such as C, N, O, P and Zr are confirmed through the occurrence of their binding energy signals at 286, 336, 535, 188 and 136 eV respectively. The amounts of elements namely C, O, N, Zr, and P are observed to be 51.12, 37.71, 1.54, 3.22 and 6.41%, respectively.

3.2 Curing Behavior of UP and $A_{0.5}ZrP$/UP

To confirm the occurrence of polymerization of UP resin even after the addition of different weight percent of $A_{0.5}ZrP$, DSC analysis was carried out from room temperature to 200 °C. Figure 7 presents the curing profile obtained from the DSC of UP and $A_{0.5}ZrP$/UP samples. There is no change in the formation of curing behavior was noticed due to the incorporation of allylamine exfoliated α-ZrP. Thus, the UP and $A_{0.5}ZrP$/UP samples show similar onset temperature at 100 °C. However, the appearance of the second peak at 138 °C in the $A_{0.5}ZrP$/UP, confirms the occurrence of polymerization of allyl group with the

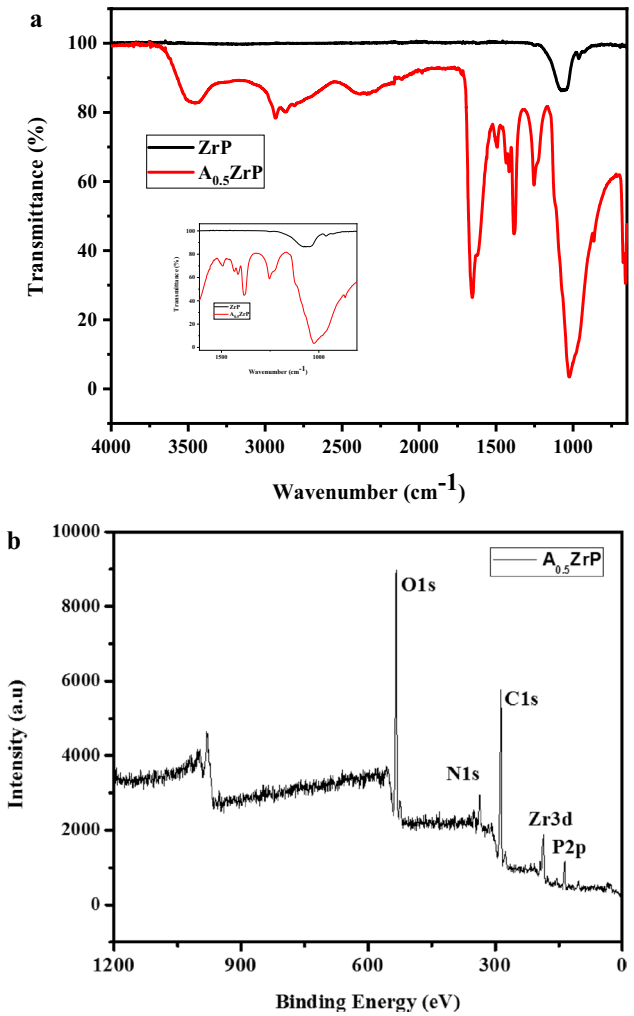

Fig. 6 **a** FTIR spectra of ZrP and allyl amine exfoliated α-ZrP. **b** XPS Spectra of allylamine exfoliated α-ZrP ($A_{0.5}ZrP$)

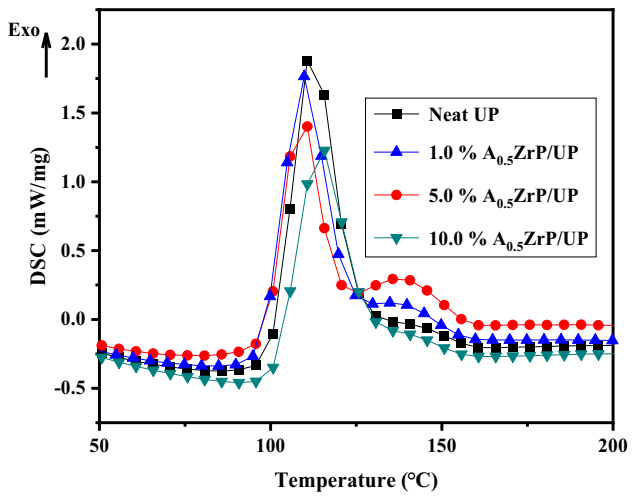

Fig. 7 DSC curing curve of the neat UP and $A_{0.5}ZrP$ reinforced UP

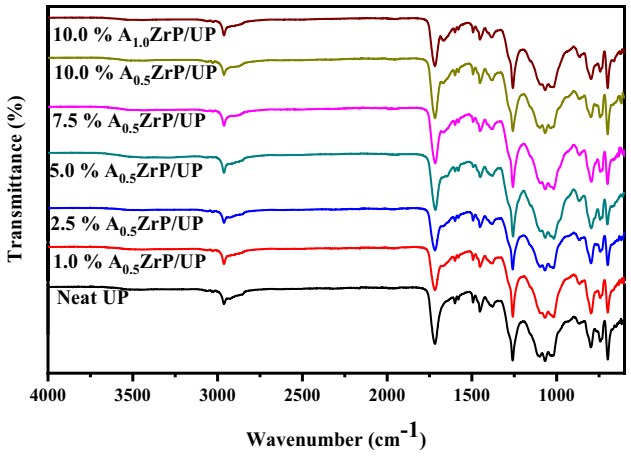

Fig. 8 FTIR Spectra of the neat UP matrix and $A_{0.5}ZrP$ reinforced UP nanocomposites

UP resin. The schematic representation of the formation $A_{0.5}ZrP$ /UP composite is presented in Fig. 1.

To validate the formation of the polymerization of the UP matrix and $A_{0.5}ZrP$/UP composite, FTIR analysis was carried and presented in Fig. 8. The appearance of bands at 2963, 1720, 1260 and 1103 cm^{-1} correspond to the $-CH_2-$, carbonyl (−C=O group of the ester bond), and C−O−C stretching vibrations respectively. Further, the bands appeared at 1444, 744 and 698 cm^{-1} corresponding to the bending vibrations of the aromatic rings [51]. In addition to the vibration bands of the UP matrix, the band at 864 cm^{-1} shown corresponds to the stretching vibrations of phosphate functional groups [52]. The presence of phosphate is highly desirable to catalyze the formation of char barriers [53]. Thus, the FTIR spectra confirm the formation of $A_{0.5}ZrP$/UP composites using low concentrated allyl amine exfoliated α-ZrP.

3.3 Mechanical Properties of UP and $A_{0.5}ZrP$/UP Matrices

Figure 9a illustrates the tensile behavior of the neat UP and $A_{0.5}ZrP$ reinforced UP nanocomposites. Initially, no significant improvement in the tensile strength was noticed upon reinforcing 1.0 and 2.5% $A_{0.5}ZrP$. However, the tensile strength value increases upon reinforcing further wt% (5.0, 7.5 and 10.0 wt%) of $A_{0.5}ZrP$. The 5.0% $A_{0.5}ZrP$/UP nanocomposite shows a 6.2% higher tensile strength than that of the neat UP matrix (Table 1). Further, incorporation of 7.5 and 10.0 wt% $A_{0.5}ZrP$ shows 37.3 and 59.4% increase in the tensile strength respectively than that of a neat UP matrix. This behavior is due to the transfer of applied stresses to the layered α-ZrP, facilitated by the interfacial adhesion between the reinforcement and matrix. Upon reinforcing excess of $A_{0.5}ZrP$ beyond 10.0 wt% shows a decrease in the tensile

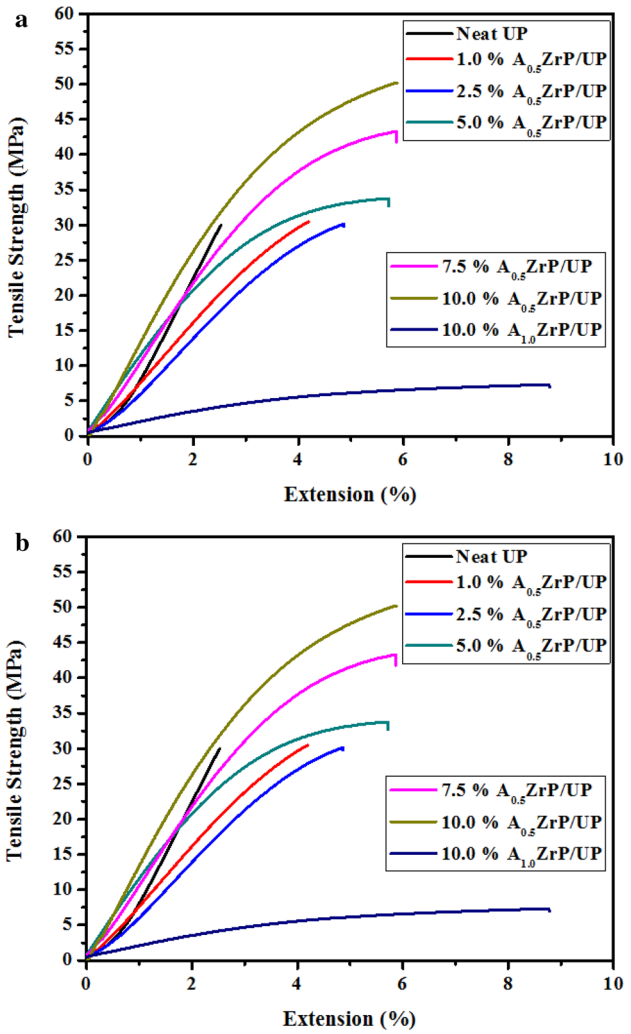

Fig. 9 **a** Tensile strength behaviour of UP matrix and A_XZrP/UP nanocomposites. **b** Flexural strength behaviour of UP matrix and A_XZrP/UP nanocomposites

strength due to the formation of brittle nature. Meantime, the tensile strength of 10.0 wt% $A_{1.0}$ZrP/UP was also measured and compared with the $A_{0.5}$ZrP/UP nanocomposites. The tensile strength decreases up to 72.2% due to the presence of aliphatic carbon chains in the resulting composite. The obtained results are interesting since earlier reports using layered MMT and Boron nitride offer only a minimal increase in tensile strength comparable to neat UP alone [2, 54].

Also, the elongation-at-break comparatively increases as the incorporation of $A_{0.5}$ZrP becomes higher. This behavior is attributed to the formation of molecular mobility with the resulting composites. During the applied force, the aliphatic chain tends to impart load transfer through mobilizing the α-ZrP hexagonal structure. Moreover, the observed flexural strength also shows significant increases with the incorporation of $A_{0.5}$ZrP (Fig. 9b, Table 1). As discussed earlier, the

Table 1 Tensile strength and flexural strength of UP matrix and A_XZrP/UP nanocomposites

Samples	Tensile strength (MPa)	Elongation at break (%)	Flexural strength (MPa)	Deformation (%)
Neat UP	29.3	2.6	100.8	1.2
1.0% $A_{0.5}$ZrP/UP	30.4	4.1	152.7	2.3
2.5% $A_{0.5}$ZrP/UP	30.6	4.8	161.4	2.3
5.0% $A_{0.5}$ZrP/UP	33.4	5.7	159.4	3.1
7.5% $A_{0.5}$ZrP/UP	43.0	5.8	159.4	3.2
10.0% $A_{0.5}$ZrP/UP	49.9	5.8	158.0	3.4
10.0% $A_{1.0}$ZrP/UP	8.7	7.3	–	–

homogeneous distribution and presence of flexible aliphatic chains contribute to the enhancement of flexural strength. Thus, the 1.0 wt% $A_{0.5}$ZrP/UP shows 51% of increment in flexural strength, whereas the 2.5 wt% $A_{0.5}$ZrP/UP increase of about 60.5%. Further, the percentage of deformation also increases, which indicates the rise in the flexibility of the network.

3.4 Thermal Properties of UP and $A_{0.5}$ZrP/UP

To study the influence of α-ZrP on the enhancement of thermal stability of UP matrices, the thermogravimetric analysis was studied. The TG curves of neat UP matrix and $A_{0.5}$ZrP reinforced UP composites are presented in Fig. 10. The thermograms of neat UP matrix and $A_{0.5}$ZrP/UP composites show similar decomposition processes. However, the initial degradation of composites with a higher concentration of $A_{0.5}$ZrP shows extensive weight losses as evidenced by the T-5% (5.0% weight loss temperature, Table 2). The initial stage degradation occurring below

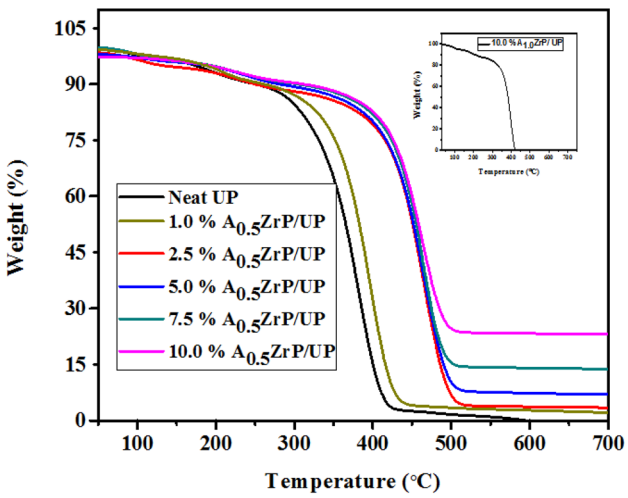

Fig. 10 TG curve of UP matrix and A_XZrP reinforced UP nanocomposites

Table 2 Thermal properties of UP matrix and A_XZrP reinforced UP nanocomposites

Samples	$T_{-5\%}$	$T_{-20\%}$	Char yield at 700 °C	LOI	UL-94
Neat UP	172	317	0	–	–
1.0% $A_{0.5}$ZrP/UP	133	333	1.3	18.0	–
2.5% $A_{0.5}$ZrP/UP	125	387	3.9	19.6	V2
5.0% $A_{0.5}$ZrP/UP	183	399	8.3	20.8	V2
7.5% $A_{0.5}$ZrP/UP	185	404	15.2	23.6	V1
10.0% $A_{0.5}$ZrP/UP	192	412	23.9	27.1	V0
10.0% $A_{1.0}$ZrP/UP	111	326	0	–	–

200 °C is attributed to the removal of moisture present in the composites. However, the temperature corresponding to the primary decomposition of UP carbon matrices was postponed to a higher temperature (from 300 to 400 °C) particularly composites with $A_{0.5}$ZrP concentration beyond 5.0 wt%. The second step degradation corresponds to the oxidation of the organic polymer networks. The composites with 10.0 wt% $A_{0.5}$ZrP exhibited a higher yield of char residue (25.3%). This is due to the presence of a homogenous concentration of reinforcement within the matrices. Besides, the inset of Fig. 10, shows the decomposition behavior of 10.0 wt% $A_{1.0}$ZrP/UP composites. The 10.0 wt% $A_{1.0}$ZrP /UP completely decomposes below the temperature 410 °C with zero char yield. This phenomenon is due to the presence of a higher concentration of allylamine and the lower amount of α-ZrP in the resulting composites.

Further, to study the flame retardant nature of the UP matric and $A_{0.5}$ZrP/UP composites, the LOI values were determined along with the performance of UL-94 rating analysis and the resulted data are presented in Table 2. The LOI value of the neat UP matrix is only 17.5% and shows no rating in the UL-94 test. The incorporation of 1.0 wt% $A_{0.5}$ZrP reinforcement results only minor difference in LOI value, thereby it also could not reach any rating in the UL-94 tests too. However, reinforcing 5.0 wt% $A_{0.5}$ZrP with UP, the LOI value significantly increased to 20.8% and attained the V-1 rating. On ignition, the propagated fire gradually drops, which also results in the formation of a minor quantity of char. Upon further incorporation of $A_{0.5}$ZrP (7.5 and 10.0 wt%), the resulting composites offer an improved LOI value of about 23.6% and 27.1% respectively. Surprisingly, the 10.0 wt% $A_{0.5}$ZrP/UP composites result in a V-0 rating with self-extinguishing behavior. The flame retardant property of the $A_{0.5}$ZrP/UP could be ascribed to the uniform distribution of ZrP within the UP matrix. The results suggested that the incorporation of layered zirconium phosphate acts as a stable barrier thus inhibits the transmission of heat into the polymer matrices

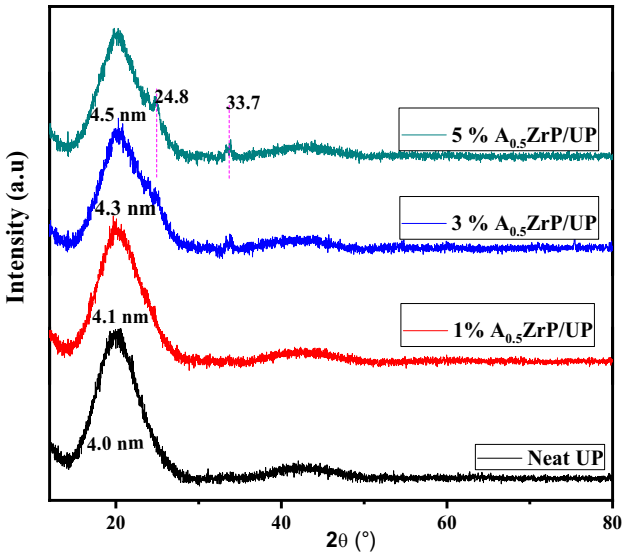

Fig. 11 XRD patterns of neat UP and $A_{0.5}$ZrP/UP nanocomposites

[55]. The observed result is in accordance with layered structure that promote the flame retardancy [56].

3.5 Diffraction Analysis of UP and $A_{0.5}$ZrP/UP Matrices

Figure 11 shows an X-ray diffractogram of a neat UP matrix and $A_{0.5}$ZrP/UP composites. The neat UP matrix shows a broad peak at 19.9°, attributed to the semi-crystalline tendency of UP matrices that arise due to the formation of molecular symmetry after polymerization [57]. Similar diffractions are also observed even after the incorporation of $A_{0.5}$ZrP into the UP matrix. Though the patterns are similar, minor changes in peak position and increase in the d spacing values of the composites are noticed with the increase in the concentration of $A_{0.5}$ZrP. As a result, the d spacing value reaches a maximum of 4.5 nm for 10.0 wt% $A_{0.5}$ZrP, whereas the neat UP shows only 4.0 nm. Besides, the composites with 10.0 wt% $A_{0.5}$ZrP shows the diffraction peak at 33.7°, which corresponds to the peak of α-ZrP. These results suggest that the presence of partially exfoliated α-ZrP within the UP matrix at higher concentration

3.6 Micrograph and Elemental Composition Analysis of UP and $A_{0.5}$ZrP/UP Matrices

Fracture surfaces observed from the SEM analysis of neat UP matric, $A_{0.5}$ZrP/UP/composites are shown in Fig. 12. The neat UP matrix displays a smooth and compact surface (Fig. 12a). The composites with a lower concentration of $A_{0.5}$ZrP (1.0 and 2.5 wt%) also show similar smooth surfaces (Fig. 12b, c). This phenomenon is due to the homogeneous

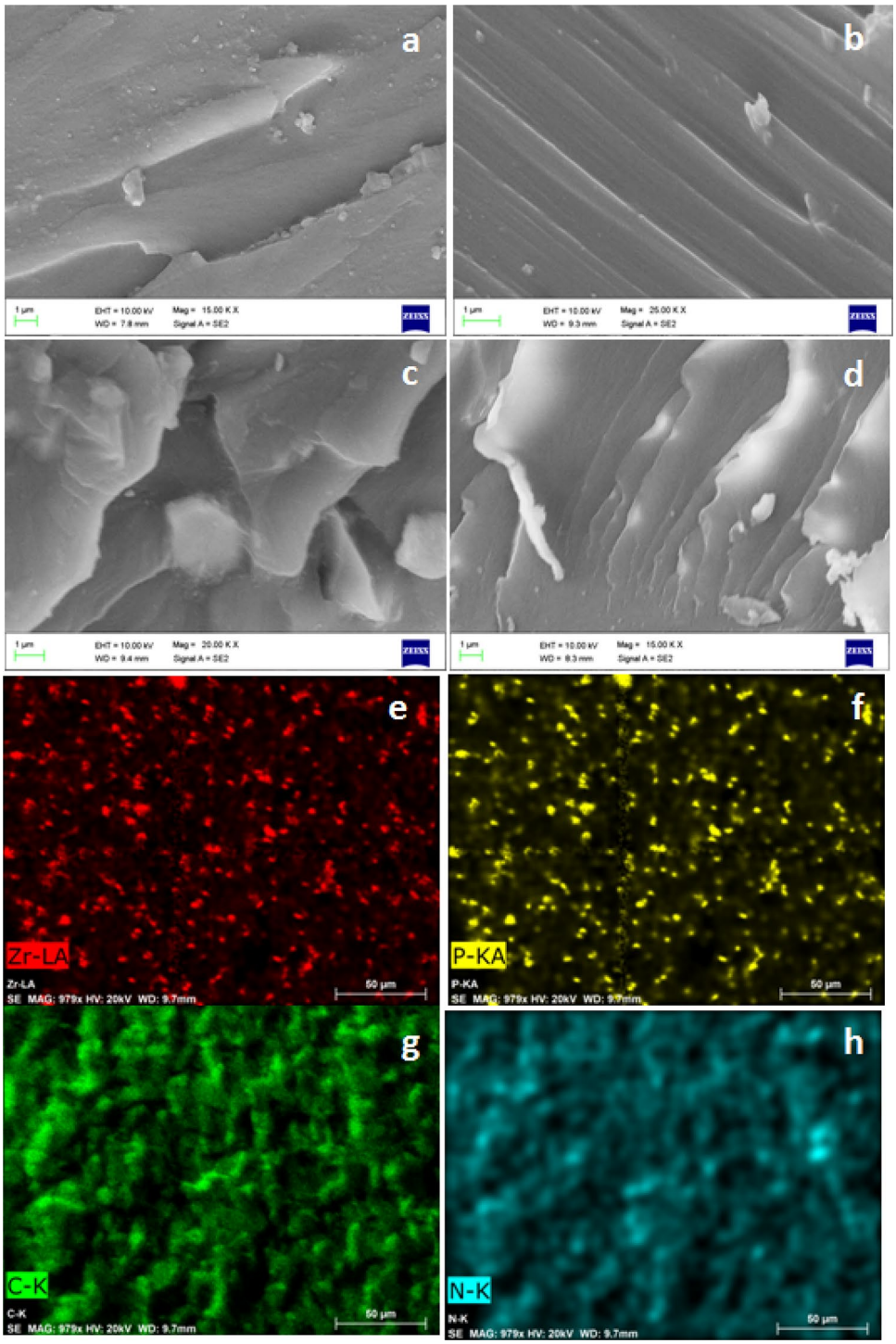

Fig. 12 FE-SEM images of fracture surfaces **a** neat UP, **b** 1.0 wt%, **c** 5.0 wt%, **d** 10.0 wt% $A_{0.5}$ZrP/UP nanocomposites and **e**–**h** elemental mapping of 10.0% $A_{0.5}$ZrP reinforced UP nanocomposites

dispersion of α-ZrP achieved through the co-polymerization. At the same time, UP composites with higher wt% (5.0 and 10.0 wt%) of $A_{0.5}$ZrP, shows rigid and rougher surfaces. The occurrence of channelized crack propagation at the interfaces during the applied forces leads to the formation of rough fracture surfaces [25, 57]. Here, the α-ZrP present within the polymer matrices performs as a covered barrier, which hinders the path of crack propagation due to strong interfacial interaction and renders high tensile strength. Figure 12e–h, shows the presence of elements such as Zr (2.81%), P (4.77%), C (56.14%), N (0.41) respectively, whereas the remaining percent attributes for the presence of O (35.87%) in the resulted composites.

Further, to ascertain the homogenous dispersion of α-ZrP at the molecular level, the TEM analysis was performed. TEM images presented in Fig. 13a–c show the two different

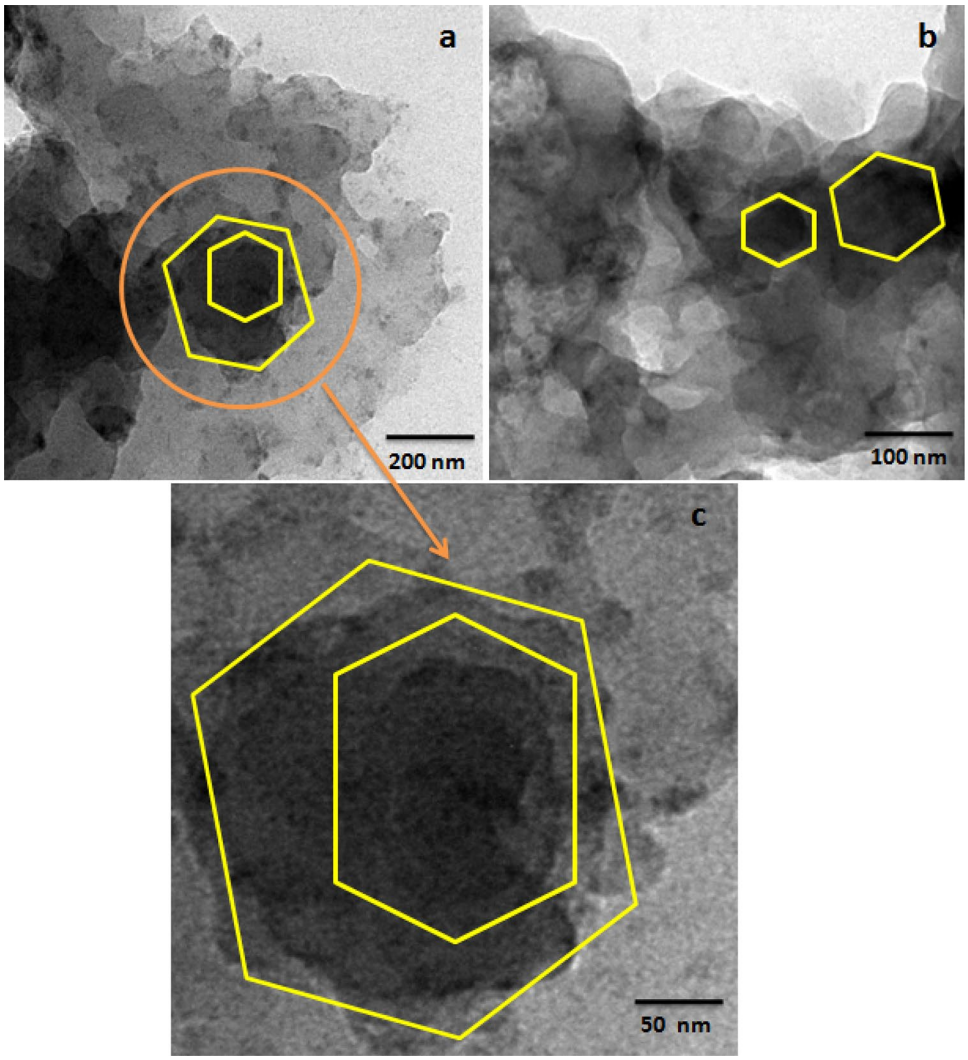

Fig. 13 **a–c** TEM images of 10.0 wt % $A_{0.5}$ZrP reinforced UP nanocomposites

sized α-ZrP particles existence in the UP matrix. The coexistence of smaller particles over the higher one in layered form confirms the partial exfoliation of α-ZrP in UP matrices (Fig. 13b). The resulting nanocomposites deliver different sizes of α-ZrP ranging from nano to micro-level as supported by SEM (Fig. 5). Thus, the α-ZrP present at the molecular level performs the catalytic activity and contributes to flame retardant behavior, in addition to the enhancement of mechanical strength.

4 Conclusions

In summary, the flame-retardant $A_{0.5}$ZrP/UP composites were prepared using different ratios of $A_{0.5}$ZrP (wt%) and studied for their thermal and mechanical properties. 10.0 wt% $A_{0.5}$ZrP reinforced UP composite exhibits an improved flame retardant nature with V-0 rating and higher thermal stability offering LOI value of about 27.1%. The catalytic action of α-ZrP favors the rapid formation of stable char with swollen mass. Similarly, the 10.0 wt% $A_{0.5}$ZrP also shows enhanced mechanical properties and better tensile strength (56%) and flexural strength (61%) due to the transfers of applied stress. Thus, the developed flame retardant AxZrP reinforced UP composites can be applied in the form of coatings, adhesives, sealants, and matrices.

Acknowledgements The authors thank the Management and the Principal, PSG institute of Technology and Applied Research for their moral and financial support.

Compliance with Ethical Standards

Conflict of interest All authors declare that they have no conflict of interest.

References

1. M.J. Hashemi, M. Jamshidi, J.H. Aghdam, Constr. Build. Mater. **163**, 767 (2018)
2. F. Laatar, M. Jayan, P. Padmanabhan, M.R. Ben, Romdhane, E. Srasra, J. Coat. Technol. Res. **15**, 293 (2018)
3. S. Jothibasu, A. Chandramohan, A.A. Kumar, M. Alagar, J. Macromol. Sci. A **55**, 433 (2018)
4. Z.A. Abdul Halim, M.A. Mat Yajid, M.H. Idris, H. Hamdan, J. Dispers. Sci. Technol. **39**, 1093 (2018)
5. Y. Cao, X.L. Wang, W.Q. Zhang, X.W. Yin, Y.Q. Shi, Y.Z. Wang, Ind. Eng. Chem. Res. **56**, 5913 (2017)
6. M. Soyama, M. Iji, Polym. J. **49**, 503 (2017)
7. K. Kanimozhi, P. Prabunathan, V. Selvaraj, M. Alagar, RSC Adv. **4**, 18157 (2014)
8. Z. Bai, L. Song, Y. Hu, R.K.K. Yuen, Ind. Eng. Chem. Res. **52**, 12855 (2013)
9. Q. Guo, H. Cheng, H. Zhang, Z. Zhong, S. Chen, J. Therm. Anal. Calorim. **135**, 2171 (2019)
10. D. Zhao, J. Wang, X.L. Wang, Y.Z. Wang, Chem. Eng. J. **344**, 419 (2018)
11. N. Amarnath, D. Appavoo, B. Lochab, ACS Sustain. Chem. Eng. **6**, 389 (2018)
12. D. Wang, Y. Kan, X. Yu, J. Liu, L. Song, Y. Hu, J. Hazard. Mater. **320**, 504 (2016)
13. M. Jiang, Y. Zhang, Y. Yu, Q. Zhang, B. Huang, Z. Chen, T. Chen, J. Jiang, J. Appl. Polym. Sci. **136**, 20 (2019)
14. G.I. Dzhardimalieva, I.E. Uflyand, J. Inorg. Organomet. Polym. Mater. **28**, 1305 (2018)
15. H. Shahrajabian, S.Y. Ahmadi-Brooghani, S.J. Ahmadi, J. Inorg. Organomet. Polym. Mater. **23**, 1282 (2013)
16. F. Ali, N. Ali, M. Altaf, A. Said, S.S. Shah, M. Bilal, J. Inorg. Organomet. Polym. Mater. (2020). https://doi.org/10.1007/s10904-020-01518-5
17. E.E. Ateia, D.E. El-Nashar, R. Ramadan, M.F. Shokry, J. Inorg. Organomet. Polym. Mater. **30**, 1041 (2019)
18. R. Rajamanikam, P. Pichaimani, M. Kumar, A. Muthukaruppan, Polym. Compos. **38**, 1881 (2017)
19. P. Prabunathan, P. Thennarasu, J.K. Song, M. Alagar, New J. Chem. **41**, 5313 (2017)
20. Y. Yu, Z. Chen, Q. Zhang, M. Jiang, Z. Zhong, T. Chen, J. Jiang, Polym. Adv. Technol. **30**, 998 (2019)
21. R.C. Zhuang, J. Yang, D.Y. Wang, Y.X. Huang, RSC Adv. **5**, 100049 (2015)
22. H. Xie, X. Lai, H. Li, X. Zeng, Appl. Clay Sci. **166**, 61 (2018)
23. E.N. Kalali, S. De Juan, X. Wang, S. Nie, R. Wang, D.Y. Wang, J. Therm. Anal. Calorim. **121**, 619 (2015)
24. H. Xiao, S. Liu, Mater. Des. **155**, 19 (2018)
25. H. Wu, C. Liu, J. Chen, Y. Yang, Y. Chen, Polym. Int. **59**, 923 (2010)
26. L. Xu, C. Lei, R. Xu, X. Zhang, F. Zhang, Polym. Degrad. Stab. **133**, 378 (2016)
27. J. Anandraj, G.M. Joshi, J. Inorg. Organomet. Polym. Mater. **27**, 1835 (2017)
28. D.R. Do Carmo, T.F.S. da Silveira, J. Inorg. Organomet. Polym. Mater. **29**, 1205 (2019)
29. L.C. Mendes, D.F. Silva, L.J.F. Araujo, A.S. Lino, J. Therm. Anal. Calorim. **118**, 1461 (2014)
30. W.J. Boo, L. Sun, J. Liu, A. Clearfield, H.J. Sue, J. Phys. Chem. C **111**, 10377 (2007)
31. F. Xia, H. Yong, X. Han, D. Sun, Nanoscale Res. Lett. **11**, 1 (2016)
32. H.-K. Lee, J.-I. Kim, J.-H. Park, T.-H. Lee, Electrochim. Acta **50**, 761 (2004)
33. H. Lu, C.A. Wilkie, M. Ding, L. Song, Polym. Degrad. Stab. **96**, 1219 (2011)
34. M. Casciola, G. Alberti, A. Donnadio, M. Pica, F. Marmottini, A. Bottino, P. Piaggio, J. Mater. Chem. **15**, 4262 (2005)
35. L. Cheng, X. Guo, C. Song, G. Yu, Y. Cui, N. Xue, L. Peng, X. Guo, W. Ding, RSC Adv. **3**, 23228 (2013)
36. Q. Wang, J. Yu, J. Liu, Z. Guo, A. Umar, L. Sun, Sci. Adv. Mater. **5**, 469 (2013)
37. B.M. Mosby, A. Díaz, V. Bakhmutov, A. Clearfield, ACS Appl. Mater. Interfaces **6**, 585 (2014)
38. K. Li, H. Lei, X. Zeng, H. Li, X. Lai, S. Chai, RSC Adv. **7**, 49290 (2017)
39. G. Cai, H. Lu, S. Xu, Z. Wang, C.A. Wilkie, Polym. Adv. Technol. **24**, 646 (2013)
40. L. Sun, W.J. Boo, H.J. Sue, A. Clearfield, New J. Chem. **31**, 39 (2007)
41. M. Casciola, G. Bagnasco, A. Donnadio, L. Micoli, M. Pica, M. Sganappa, M. Turco, Fuel Cells **9**, 394 (2009)
42. P. Prabunathan, A. Vasanthakumar, M. Manoj, A. Hariharan, M. Alagar, J. Polym. Res. **27**, 1 (2020)
43. N. Lu, K.Y. Lin, C.C. Kung, J.W. Jhuo, Y. Zhou, J. Liu, L. Sun, RSC Adv. **4**, 27329 (2014)
44. M. Shuai, A.F. Mejia, Y.W. Chang, Z. Cheng, CrystEngComm **15**, 1970 (2013)
45. Y.H. Yu, Y.P. Chen, M. Zeng, Z. Cheng, Mater. Lett. **163**, 158 (2016)
46. B.R. Selvan, K. Dasthaiah, A.S. Suneesh, K.A. Venkatesan, M.P. Antony, R.L. Gardas, Radiochim. Acta **105**, 275 (2017)
47. L. Sun, W.J. Boo, R.L. Browning, H.-J. Sue, A. Clearfield, Chem. Mater. **17**, 5606 (2005)
48. Y. Zhang, X. Zeng, H. Li, X. Lai, Y. Guo, R. Zheng, Mater. Lett. **174**, 230 (2016)
49. Y.-H. Yu, X. Wang, A. Shinde, Z. Cheng, J. Vis. Exp. **111**, e53511 (2016)
50. X. Wu, Y. Tao, J. Hong, J. Mater. Chem. **14**, 901 (2004)
51. K. Kanimozhi, P. Prabunathan, V. Selvaraj, M. Alagar, Polym. Compos. **35**, 1663 (2014)
52. M.V. Ramos-Garcés, J. Sanchez, K. La Luz-Rivera, D.E. Del Toro-Pedrosa, T.F. Jaramillo, J.L. Colón, Dalton Trans. **49**, 3892 (2020)
53. D. Yang, Y. Hu, L. Song, S. Nie, S. He, Y. Cai, Polym. Degrad. Stab. **93**, 2014 (2008)
54. F. Chu, D. Zhang, Y. Hou, S. Qiu, J. Wang, W. Hu, L. Song, ACS Appl. Mater. Interfaces **10**, 40168 (2018)
55. Y. Zhang, X. Zeng, X. Lai, H. Li, RSC Adv. **8**, 111 (2018)
56. Y. Hai, S. Jiang, X. Qian, S. Zhang, P. Sun, B. Xie, N. Hong, J. Colloid Interface Sci. **509**, 285 (2018)
57. C. Liu, Z. Wang, Y. Huang, H. Xie, Z. Liu, Y. Chen, W. Lei, L. Hu, Y. Zhou, R. Cheng, RSC Adv. **3**, 22380 (2013)